A Sufficient Condition on Convex Relaxation of AC Optimal Power Flow in Distribution Networks

Shaojun Huang, *Student Member, IEEE*, Qiuwei Wu, *Senior Member, IEEE*, Jianhui Wang, *Senior Member, IEEE*, and Haoran Zhao, *Member, IEEE*

***Abstract*—This paper proposes a sufficient condition for the convex relaxation of ac optimal power flow (OPF) in radial distribution networks as a second order cone program (SOCP) to be exact. The condition requires that the allowed reverse power flow is only reactive or active, or none. Under the proposed sufficient condition, the feasible sub-injection region (power injections of nodes excluding the root node) of the ac OPF is convex. The exactness of the convex relaxation under the proposed condition is proved through constructing a group of monotonic series with limits, which ensures that the optimal solution of the SOCP can be converted to an optimal solution of the original ac OPF. The efficacy of the convex relaxation to solve the ac OPF is demonstrated by case studies of an optimal multi-period planning problem of electric vehicles in distribution networks.**

***Index Terms*—AC optimal power flow (AC OPF), convex relaxation, convexity, electric vehicle (EV), power distribution network, second order cone program (SOCP).**

NOMENCLATURE

Sets

$\mathcal{E}$	Set of edges of the whole network.
$\mathcal{E}_i$	Set of edges of the subtree from node i. i
$\mathcal{N}$	Set of nodes of the whole network.
$\mathcal{N}^+$	Subset of nodes, excluding node 0, named as plus nodes.
$\mathcal{N}_i$	Set of nodes of the subtree from node i. i
$\mathcal{N}_i^+$	Subset of nodes of the subtree, excluding node i.
$\mathcal{P}$	Feasible (active) injection region of the OPF.
$\mathcal{P}^+$	Feasible (active) sub-injection region of the OPF.
$\mathcal{S}$	Feasible injection region of the OPF.
$\mathcal{S}^+$	Feasible sub-injection region of the OPF.
$\tilde{\mathcal{S}}$	Feasible injection region of the SOCP.
$\tilde{\mathcal{S}}^+$	Feasible sub-injection region of the SOCP.
$\mathcal{T}$	Set of planning periods.
$\mathbb{V}$	Set of EVs.
$\mathbb{V}_i$	Set of EVs connected to node i.
$\mathbb{Z}$	Set of positive integer numbers.
$\mathbb{Z}^-$	Set of negative integer numbers.

Parameters

a_{kt}	EV availability.
b_{it}	Conventional consumption, complex number.
c_t	Energy price.
$\bar{e}_k$	EV charging power upper limit, active power.
$\bar{i}$	(Square of the magnitude) line current upper limit.
r	Resistance.
$\bar{p}$	Real part of $\bar{s}$.
$\bar{q}$	Imaginary part of $\bar{s}$.
$\bar{s}$	Upper limit of the sub-injection.
$\underline{s}$	Lower limit of the sub-injection.
x	Reactance.
v_0	(Square) voltage of node 0, real number.
$\underline{v}_i$	(Square) voltage of plus nodes, lower limit.
$\bar{v}_i$	(Square) voltage of plus nodes, upper limit.
z	Impedance, $z = r + jx$.
$\bar{S}$	Line capacity (absolute value) upper limit.

Variables

e	EV charging power, active power.
i	(Square of the magnitude) line current.
p, p_i	Real part of s.
p_0	Real part of s_0.
q, q_i	Imaginary part of s.
s, s_i	Injection of plus nodes ($i > 0$), i.e. sub-injection.
s_0	Injection of node 0, complex number.
v, v_i	(Square) voltage of plus nodes, real number, $i > 0$.
$\hat{v}_i$	Linear approximation of (square) voltage.
P	Reverse line flow, active part.
$\hat{P}$	Linear approximation of the reverse line flow, active part.
Q	Reverse line flow, reactive part.
$\hat{Q}$	Linear approximation of the reverse line flow, reactive part.
S	Reverse line flow, complex number.
$\hat{S}$	Linear approximation of the reverse line flow, complex number.

I. INTRODUCTION

OPTIMAL power flow (OPF) is a very important optimization problem widely used in power engineering

Manuscript received December 14, 2015; revised March 9, 2016 and April 20, 2016; accepted May 28, 2016. Date of publication May 18, 2016; date of current version February 16, 2017. The work was supported by the EU Seventh Framework Programme (FP7) through the "Ideal Grid for All (IDE4L)" project. The work of S. Huang was carried out during his Ph.D. external stay in the Center for Information Technology Research in the Interest of Society (CITRIS), University of California, Berkeley, CA, USA, in 2015. Paper no. TPWRS-01780-2015.

S. Huang, Q. Wu and H. Zhao are with the Center for Electric Power and Energy, Department of Electrical Engineering, Technical University of Denmark, 2800 Kgs. Lyngby, Denmark (e-mail: shuang@elektro.dtu.dk; qw@elektro.dtu.dk; hzhao@elektro.dtu.dk).

J. Wang is with the Argonne National Laboratory, Argonne, IL 60439 USA (e-mail: jianhui.wang@anl.gov).

Digital Object Identifier 10.1109/TPWRS.2016.2574805

applications, such as congestion management, economic operation and control. The OPF considers the economic aspect of the power system components, and models the system at the steady state. There are two types of OPF, i.e. AC OPF [1] and DC OPF [2], resulting from AC and DC power flow models.

The DC OPF is a linear problem, and can be solved very efficiently and robustly by many commercial optimization solvers such as GAMS/CPLEX [3]. However, the solution of the DC OPF is only an approximation of the power system status. It is far from accurate if the *R*/*X* ratio is high in the studied system.

The AC OPF is non-convex in its original form and is an NP-hard problem. General-purpose nonlinear programming solvers can be used to solve the AC OPF. A number of dedicated methods were developed to solve the AC OPF problems in the last two decades, such as the trust region interior point algorithm [4], [5], Lagrangian method [6], and primal-dual interior point method [7]. However, these methods normally obtain a locally optimal solution and it is not possible to know how far it is from the global optimum.

The convex relaxation method for solving the AC OPF was first presented in [8] as a second-order cone program (SOCP) for radial networks and in [9] as a semidefinite programming (SDP) for meshed networks. For meshed networks, [10] has analyzed the exactness of the convex relaxation. However, the analysis is limited to resistive networks.

For radial networks, [11]–[13] have proposed several sufficient conditions for the convex relaxation to be exact. In [11], [12], it is proposed that if just one of any two connected nodes has a lower active power bound and no node has a lower reactive power bound, the convex relaxation is exact. However, these sufficient conditions may not be practical. In [13], the authors propose that if the upper bounds of the active and reactive power are not too large, the convex relaxation will be exact. The conclusion of [13] is promising as it allows a certain amount of feed-in power from renewables; however, the constraints of the AC OPF formulation in [13] miss the thermal and line capacity limits. The line capacity limit may lead to inexactness of the convex relaxation of the AC OPF as shown in [14]. Besides, the thermal and line capacity limits are necessary in many practical applications with renewable energies or flexible demands present, such as the congestion management applications in [15], [16]. The details of the convex relaxation for the AC OPF can be found in [17], [18].

This paper proposes a sufficient condition, denoted as C1 and described in Section III, such that the convex relaxation of the AC OPF with all practical constraints is exact. The main contributions of this paper can be summarized as follows: (a) Prove that under condition C1, the feasible sub-injection region (feasible power injections to the nodes excluding the root node) of the AC OPF is the same as the feasible sub-injection region of the SOCP, and both are convex. (b) Relax the requirement of the cost function from being strictly increasing to non-decreasing. (c) Prove C1 is a sufficient condition leading to exact convex relaxation of the AC OPF with current, voltage and line capacity constraints. (d) Analyze the sufficient condition for exact convex relaxation of OPF with intertemporal constraints, and demonstrate the efficacy of the convex relaxation for solving the AC OPF of multi-period energy planning of electrical vehicles (EVs).

The paper is organized as follows. Section II discusses the convexity of the sub-injection region under condition A1, which is straightforward but more conservative than C1. Section III analyzes the exactness of the convex relaxation under condition C1. In Section IV, the AC OPF with multi-period energy planning of EVs is described and analyzed. Case studies of the AC OPF with EV planning are presented and discussed in Section V, followed by conclusions.

II. Convexity and Convex Relaxation of AC OPF in Distribution Networks

A. Convex Relaxation

A few assumptions are made for the convexity analysis and convex relaxation of AC OPF in distribution networks. Only radial networks are considered, i.e. the network $(\mathcal{N}, \mathcal{E})$ is a tree. Node 0 is chosen to be the slack node, i.e. voltage v_0 is fixed and given (normally 1 p.u.). Node 0 is also the root of the tree graph and the direction of each edge is pointed towards the root. In all practical applications in distribution networks, the voltage limits of each node are $1 \pm \alpha\%$ p.u., where α can be a number between 4 and 10 depending on the standards. Therefore, it is reasonable to assume that $\bar{v} > v_0$ and $\underline{v} < v_0$ (assume that $v_0 = 1$ p.u.).

The original AC OPF can be written as (1)–(9). The function f_0 is listed separately in the objective function because there is a special requirement for f_0 (see discussion in Section III-A). Constraints (2)–(5) describe the line flow through a branch flow model. Constraints (6) and (7) are the thermal and line capacity limits. Constraint (8) is the limit of the generator output or the demand, and (9) is the voltage limits.

$$\mathbf{OPF}: \min_{s,S,v,i,s_0} f_0(\mathrm{Re}(s_0)) + f_1(\mathrm{Re}(s)), \tag{1}$$

s.t.

$$S_{ij} = s_i + \sum_{h:h\to i} (S_{hi} - z_{hi} i_{hi}), \qquad \forall (i,j) \in \mathcal{E}, \tag{2}$$

$$0 = s_0 + \sum_{h:h\to 0} (S_{h0} - z_{h0} i_{h0}), \tag{3}$$

$$v_i - v_j = 2\mathrm{Re}(\bar{z}_{ij} S_{ij}) - |z_{ij}|^2 i_{ij}, \quad \forall (i,j) \in \mathcal{E}, \tag{4}$$

$$i_{ij} = \frac{|S_{ij}|^2}{v_i}, \qquad \forall (i,j) \in \mathcal{E}, \tag{5}$$

$$i_{ij} \le \bar{i}_{ij}, \qquad \forall (i,j) \in \mathcal{E}, \tag{6}$$

$$|S_{ij}| \le \bar{S}_{ij}, \qquad \forall (i,j) \in \mathcal{E}, \tag{7}$$

$$\underline{s}_i \le s_i \le \bar{s}_i, \qquad \forall i \in \mathcal{N}^+, \tag{8}$$

$$\underline{v}_i \le v_i \le \bar{v}_i, \qquad \forall i \in \mathcal{N}^+. \tag{9}$$

Its convex relaxation as an SOCP is shown below [19].

SOCP: (1) s.t. (2)–(4), (6)–(9), and

$$i_{ij} \ge \frac{|S_{ij}|}{V_i}, \forall (i,j) \in \varepsilon. \tag{10}$$

To clearly show the fundamental idea of the convex relaxation as an SOCP, condition A1 is introduced first.

A1: The upper limit of the sub-injection fulfils: $\bar{s} \leq 0$.

Though A1 is a special case of the condition proposedin [13], it needs to be proven to be a sufficient condition since the AC OPF has current and line capacity constraints compared to the one in [13].

The physical meaning of A1 is that all the nodes except the root will draw active and/or reactive power from the system. This condition is easy to understand and can be used in many applications where the generation from, e.g. renewable energy sources, is less than the consumption.

B. Convexity of Sub-Injection Region

Before studying the exactness of the convex relaxation of the AC OPF, it is helpful to know more of the structure of the AC OPF. As shown in [11], [12], the feasible set $\mathcal{P}$, known as the feasible injection region, is normally non-convex. However, if the focus is put on the feasible injection region of p (active power injection of plus nodes $\mathcal{N}^+$, real part of s), the feasible set can be proven to be convex. This partial injection region can be named as the feasible sub-injection region, $\mathcal{P}^+$, (the word "feasible" is omitted later on for brevity). Set $\mathcal{P}^+$ is an orthogonal projection of $\mathcal{P}$ to the subspace of vector p

$$\begin{aligned}\mathcal{P} &= \{p_0, p:\ (2)-(9)\}\\ \mathcal{P}^+ &= \{(2)-(9)\}.\end{aligned}$$

In fact, a stronger statement regarding the sub-injection region with reactive power included, i.e. $\mathcal{S}^+$, can be made

$$\begin{aligned}\mathcal{S} &= \{s_0, s:\ (2)\text{–}(9)\}\\ \mathcal{S}^+ &= \{s:\ (2)\text{–}(9)\}.\end{aligned}$$

Proposition 1: $\mathcal{S}^+$ is convex if A1 holds.

The idea of focusing on the sub-injection region comes from the power flow calculation methods, such as the Newton-Raphson method or Forward-Backward method. In the power flow calculations, the power injection of the slack node is dependent on the power injections of other nodes, i.e. the sub-injection. In other words, only the sub-injections are free variables while the injection of node 0 is not. Since not all variables are free ones, $\mathcal{P}$ or $\mathcal{S}$ is not convex unless the relationships between these variables are linear, which is not true because of (5). Therefore, it is reasonable to put the focus on the sub-injection.

Proposition 1 will be proven after the proof of the following lemma.

Lemma 1: If A1 holds, then $\mathcal{S}^+ = \tilde{\mathcal{S}}^+$, i.e. the sub-injection region is equal to the convex-relaxed one

$$\begin{aligned}\tilde{\mathcal{S}} &= \{s_0, s:\ (2)-(4),\ (6)-(10)\}\\ \tilde{\mathcal{S}}^+ &= \{s:\ (2)-(4),\ (6)-(10)\}.\end{aligned}$$

It is obvious that $\forall s \in \mathcal{S}^+$, then $s \in \tilde{\mathcal{S}}^+$ because of the relaxation. Therefore, there is $\mathcal{S}^+ \subseteq \tilde{\mathcal{S}}^+$. Then we only need to prove $\mathcal{S}^+ \supseteq \tilde{\mathcal{S}}^+$.

$\forall s \in \tilde{\mathcal{S}}^+$, $\exists (S^{(0)}, v^{(0)}, i^{(0)}, s_0^{(0)})$ such that $(s, S^{(0)}, v^{(0)}, i^{(0)}, s_0^{(0)})$ satisfies (2)–(4), (6)–(10). Then employ the following iteration method to construct a series of variables $(S^{(k)}, v^{(k)}, i^{(k)}, s_0^{(k)})$.

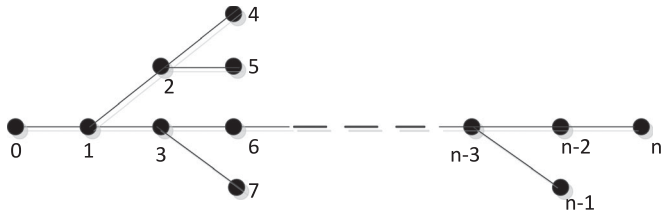

Fig. 1. Relabel the nodes according to their depth.

Reorganize the tree network as shown in Fig. 1 according to the depth (the distance to the root) of the nodes. Relabel the node number such that the deeper the node, the larger the number. In case of the same depth, the numbering is arbitrary.

Let $(S^{(k)}, v^{(k)}, i^{(k)}, s_0^{(k)}) = (S^{(0)}, v^{(0)}, i^{(0)}, s_0^{(0)}) \quad \forall k \in \mathbb{Z}^-$, and ${v_0}^{(k)} = v_0$. Then in the k-th ($k > 0$) iteration, apply a Forward-Backward sweep algorithm as described below.

Forward: For $i = n, n-1, n-2, \ldots, 1$, and $(i,j) \in \mathcal{E}$, apply sequentially,

$$\begin{aligned}{S_{ij}}^{(k)} &= s_i + \sum_{h:h\to i} \left({S_{hi}}^{(k)} - z_{hi}{i_{hi}}^{(k)}\right)\\ &\geq s_i + \sum_{h:h\to i} \left({S_{hi}}^{(k-1)} - z_{hi}{i_{hi}}^{(k-1)}\right)\\ &= {S_{ij}}^{(k-1)}, \qquad (11)\end{aligned}$$

$${i_{ij}}^{(k)} = \frac{\left|{S_{ij}}^{(k)}\right|^2}{{v_i}^{(k-1)}} \leq \frac{\left|{S_{ij}}^{(k-1)}\right|^2}{{v_i}^{(k-1)}} \leq \frac{\left|{S_{ij}}^{(k-1)}\right|^2}{{v_i}^{(k-2)}} \leq {i_{ij}}^{(k-1)}. \qquad (12)$$

For node 0,

$$\begin{aligned}{s_0}^{(k)} &= -\sum_{h:h\to 0} \left({S_{h0}}^{(k)} - z_{h0}{i_{h0}}^{(k)}\right)\\ &\leq -\sum_{h:h\to 0} \left({S_{h0}}^{(k-1)} - z_{h0}{i_{h0}}^{(k-1)}\right)\\ &= {s_0}^{(k-1)}. \qquad (13)\end{aligned}$$

Backward: For $i = 1, 2, 3, \ldots, n-1, n$, and $(i,j) \in \mathcal{E}$, apply,

$$\begin{aligned}{v_i}^{(k)} &= {v_j}^{(k)} + 2\,\mathrm{Re}(\bar{z}_{ij}{S_{ij}}^{(k)}) - |z_{ij}|^2{i_{ij}}^{(k)}\\ &\geq {v_j}^{(k-1)} + 2\,\mathrm{Re}(\bar{z}_{ij}{S_{ij}}^{(k-1)}) - |z_{ij}|^2{i_{ij}}^{(k-1)}\\ &= {v_i}^{(k-1)}. \qquad (14)\end{aligned}$$

The above algorithm not only shows how to update the variables iteratively, but also ensures that the obtained series are monotonic.

In order to show the monotone of the series, let $k = 1$. Since $\forall i > 0$, j is unique such that $(i,j) \in \mathcal{E}$, the subscription j is sometimes omitted in branch variables or parameters for brevity. In the forward sweep, when $i = n$, the inequality in (11) holds because it is a leaf node. Because $s_n \leq 0$ due to A1, ${S_n}^{(1)} \leq 0$. Therefore, the first inequality in (12) holds due to (11).

Because $v^{(k)} = v^{(0)} \quad \forall k \leq 0 \; \forall k \leq 0$, the second inequality in (12) holds. According to (10), ${i_n}^{(0)} \geq |{S_n}^{(0)}|^2/{v_n}^{(0)}$, the third inequality in (12) holds as well. When $i = n-1$, the inequality in (11) holds because (11) and (12) holds for any of its child nodes (if any) with the relabeling shown in Fig. 1. Noticing that for any of its child nodes (if any), ${S_{h,n-1}}^{(1)} \leq 0$, $z_{h,n-1} \geq 0$ and ${i_{h,n-1}}^{(0)} \geq 0$, there is ${S_{n-1}}^{(1)} \leq 0$. With (11) and ${S_{n-1}}^{(1)} \leq 0$, the first inequality in (12) holds. Similar to the analysis for $i = n$, the second and third inequality in (12) holds for $i = n-1$. Similarly, it can be verified that (11) and (12) hold for the rest i. The analysis of (13) is the same as (11).

In the backward sweep, when $i = 1$, the inequality holds in (14) because ${v_0}^{(1)} = v_0$, (11) and (12). When $i > 1$, with the relabeling shown in Fig. 1, ${v_j}^{(1)}$ is always determined before ${v_i}^{(1)}$ and ${v_j}^{(1)} \geq {v_j}^{(0)}$ due to (14). Therefore, the inequality in (14) holds for $i = 2, 3, ..., n-1, n$, respectively. The second equation in (11), (13) and (14) holds because (2)–(4) hold for $(s, S^{(0)}, v^{(0)}, i^{(0)}, s_0^{(0)})$.

Because of the iterative nature of (11)–(14), it can be verified that they hold for $k = 2, 3, 4, \ldots$. Therefore, there exists the following monotonic series:

$$\{S^{(k)}\} : S^{(0)} \leq S^{(1)} \leq S^{(2)} \leq \cdots \leq 0$$
$$\{i^{(k)}\} : i^{(0)} \geq i^{(1)} \geq i^{(2)} \geq \cdots \geq 0$$
$$\{{s_0}^{(k)}\} : {s_0}^{(0)} \geq {s_0}^{(1)} \geq {s_0}^{(2)} \geq \cdots \geq 0$$
$$\{v^{(k)}\} : v^{(0)} \leq v^{(1)} \leq v^{(2)} \leq \cdots \leq v_0.$$

In the last series, v_0 is a bound, because $2\mathrm{Re}(\bar{z}_{ij}{S_{ij}}^{(k)}) - |z_{ij}|^2 {i_{ij}}^{(k)} \; -|z_{ij}|^2 {i_{ij}}^{(k)}$ in (14) is negative. Since all the above infinite monotonic series have bounds, they have limits. Denote $S^* = \lim_{k\to+\infty} S^{(k)}$, $i^* = \lim_{k\to+\infty} i^{(k)}$, ${s_0}^* = \lim_{k\to+\infty} {s_0}^{(k)}$ and $v^* = \lim_{k\to+\infty} v^{(k)}$.

It can be verified that $(s, S^*, v^*, i^*, {s_0}^*)$ fulfills the line flow constraints (2)–(5) and s satisfies (8). It can also be shown that (S^*, v^*, i^*) satisfies constraints (6), (7) and (9) because of the assumption of $(S^{(0)}, v^{(0)}, i^{(0)})$ and the relation between $(S^{(0)}, v^{(0)}, i^{(0)})$ and (S^*, v^*, i^*). Hence, $(s, {s_0}^*) \in \mathcal{S}$ and $s \in \mathcal{S}^+$. This means $\mathcal{S}^+ \supseteq \tilde{\mathcal{S}}^+$. It ends the proof of Lemma 1.

With Lemma 1 proved, Proposition 1 is easy to be proved because $\tilde{\mathcal{S}}^+$ is convex since it is an orthogonal projection of the convex set $\tilde{\mathcal{S}}$. Therefore, $\mathcal{S}^+$ is convex as well.

III. Exactness Analysis

A. Exactness of Convex Relaxation

In [13], a definition of the exactness of the convex relaxation is given as: the SOCP is exact if every of its optimal solutions satisfies the nonlinear line flow constraint (5). This requires (10) to be active at the optimal point and f_0 to be strictly increasing. However, this requirement can be relaxed.

It can be seen from the proof of Lemma 1 that any optimal point of the SOCP can be converted to a feasible point to the original AC OPF. In order to use this Lemma, the definition of the convex relaxation exactness is modified to an intuitive one: the SOCP is exact if the gap between the optimal values of the AC OPF and its convex relaxation is zero. It is shown below that f_0 is only required to be non-decreasing for the SOCP to be exact.

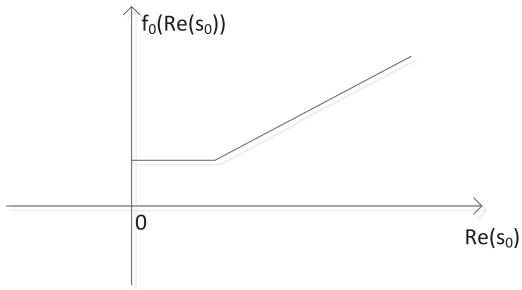

Fig. 2. An example of non-decreasing function f_0.

Proposition 2: When f_0 is non-decreasing, the SOCP is exact if A1 holds.

Proof: Assume that (s^*, s_0^*) is an optimal solution of the SOCP and the constructed feasible point of the AC OPF is (s^*, s_0^{**}), where s_0^{**} is the constructed feasible injection at node 0 using the Forward-Backward sweep method described in Section II-B. It is obvious that,

$$\mathtt{f}_0(\mathrm{Re}(s_0^*)) + \mathtt{f}_1(\mathrm{Re}(s^*)) \leq \mathtt{f}_0(\mathrm{Re}(s_0^{**})) + \mathtt{f}_1(\mathrm{Re}(s^*)),$$

because (s^*, s_0^*) is an optimal point of the SOCP. It is known from the construction process that $s_0^{**} \leq s_0^*$. Therefore, if f_0 is non-decreasing, there is,

$$\mathtt{f}_0(\mathrm{Re}(s_0^*)) + \mathtt{f}_1(\mathrm{Re}(s^*)) \geq \mathtt{f}_1(\mathrm{Re}(s_0^{**})) + \mathtt{f}_1(\mathrm{Re}(s^*)).$$

Therefore, they are equal. It is obvious that (s^*, s_0^{**}) is an optimal solution of the AC OPF and it has the same optimal value. This ends the proof of Proposition 2.

An example of non-decreasing function f_0 is shown in Fig. 2. In fact, f_0 can be zero or constant, which is a special case of non-decreasing. In that case, the SOCP is equivalent to the AC OPF in terms of having the same sub-injection region and the same objective value for every feasible point. The significance of this argument can be seen from the EV planning application presented in [20], [21]. The charging service provider employs an OPF problem to make an optimal charging plan for the EVs with the network constraint information received from the DSO. The optimal planning considers only the cost of EV charging; therefore, the cost function f_0 is zero in this application. The authors of [20], [21] use an iterative method to solve the ACOPF problem, which is slow and complicated. However, employ the method proposed in this paper, this application can be solved more efficiently (see Sections IV and V).

B. The Proposed Sufficient Condition for Exactness

A new sufficient condition, denoted as C1, is proposed in this paper, which also ensures an exact convex relaxation and a convex sub-injection region, but much wider applicability.

C1: The sub-injection s satisfies (15)–(18)

$$\hat{S}_{ij} = s_i + \sum_{h:h\to i} \hat{S}_{hi}, \quad \forall (i,j) \in \mathcal{E}, \tag{15}$$

$$\hat{v}_i - \hat{v}_j = 2\mathrm{Re}(\bar{z}_{ij}\hat{S}_{ij}), \quad \forall (i,j) \in \mathcal{E}, \tag{16}$$

$$\mathrm{Re}(\bar{z}_{ht}\hat{S}_{ij}) \le 0, \quad \forall (i,j) \in \mathcal{E}, (h,t) \in \mathcal{E}_i, \tag{17}$$

$$\hat{v}_i \le \bar{v}_i, \quad \forall i \in \mathcal{N}^+. \tag{18}$$

In (16), $\hat{v}_0 = v_0$. Equations (15) and (16) are known as Linear Distribution Flow Model [22]. It can be verified that A1 is a special case of C1 (see Section III-C). Notice that the linear approximation of the voltage ($\hat{v}$) and the reverse power ($\hat{S}$) is an upper bound of the actual voltage (v) and reverse power (S). The physical meaning of (17) can be interpreted as that the network does not allow both active and reactive reverse power flow simultaneously on its non-leaf lines (neither of the line ends is a leaf node). C1 is suitable for the applications with light reverse power flow, such as EV planning problems with reactive power support functions or with capacitor banks (see the case study in Section V-C). Equation (18) will be always satisfied if the reverse power flow is not heavy.

Proposition 3: When f_0 is non-decreasing, the SOCP is exact if C1 holds.

Proof: In order to prove the exactness of the SOCP, the key is to check the monotone of the constructed series, $\{S^{(k)}\}$, $\{i^{(k)}\}$, $\{{s_0}^{(k)}\}$, $\{v^{(k)}\}$, using the Forward-Backward sweep method.

With $k=1$, for $i = n, n-1, n-2, \ldots, 1$, and $(i,j) \in \mathcal{E}$, there is,

$$\begin{aligned}
\Delta S_{ij} &= {S_{ij}}^{(1)} - {S_{ij}}^{(0)} = \sum_{(h,t)\in\mathcal{E}_i} (-z_{ht}({i_{ht}}^{(1)} - {i_{ht}}^{(0)}) \\
&= \sum_{(h,t)\in\mathcal{E}_i} (-z_{ht}\Delta i_{ht}) \\
&\ge 0 \qquad (19)\\
\Delta|S_{ij}|^2 &= \left|{S_{ij}}^{(1)}\right|^2 - \left|{S_{ij}}^{(0)}\right|^2 = ({P_{ij}}^{(1)})^2 + ({Q_{ij}}^{(1)})^2 \\
&\quad -({P_{ij}}^{(0)})^2 - ({Q_{ij}}^{(0)})^2 \\
&= (\Delta P_{ij})({P_{ij}}^{(1)} + {P_{ij}}^{(0)}) \\
&\quad +(\Delta Q_{ij})({Q_{ij}}^{(1)} + {Q_{ij}}^{(0)}) \\
&\le (\Delta P_{ij})(2\hat{P}_{ij}) + (\Delta Q_{ij})(2\hat{Q}_{ij}) \\
&= 2\left(\sum_{(h,t)\in\mathcal{E}_i} -r_{ht}\Delta i_{ht}\right)\hat{P}_{ij} + \qquad (20)\\
&\quad 2\left(\sum_{(h,t)\in\mathcal{E}_i} -x_{ht}\Delta i_{ht}\right)\hat{Q}_{ij} \\
&= 2\sum_{(h,t)\in\mathcal{E}_i} -\Delta i_{ht}(r_{ht}\hat{P}_{ij} + x_{ht}\hat{Q}_{ij}) \le 0
\end{aligned}$$

$$\begin{aligned}
\Delta i_{ij} = {i_{ij}}^{(1)} - {i_{ij}}^{(0)} &\le \frac{\left|{S_{ij}}^{(1)}\right|^2}{{v_i}^{(0)}} - \frac{\left|{S_{ij}}^{(0)}\right|^2}{{v_i}^{(-1)}} \\
&\le \frac{\left|{S_{ij}}^{(1)}\right|^2 - \left|{S_{ij}}^{(0)}\right|^2}{{v_i}^{(0)}} = \frac{\Delta|S_{ij}|^2}{{v_i}^{(0)}} \le 0. \qquad (21)
\end{aligned}$$

Equations (19)–(21) can be verified sequentially, i.e. after verify all of them for $i = n$, start over again to verify (19)–(21) for $i = n-1$. For node 0, there is,

$$\begin{aligned}
\Delta s_0 &= {s_0}^{(1)} - {s_0}^{(0)} = \sum_{ht\in\mathcal{E}} z_{ht}({i_{ht}}^{(1)} - {i_{ht}}^{(0)}) \\
&= \sum_{ht\in\mathcal{E}} z_{ht}\Delta i_{ht} \\
&\le 0 \qquad (22)
\end{aligned}$$

For $i = 1, 2, 3, \ldots, n-1, n$ and $(i,j) \in \mathcal{E}$,

$$\begin{aligned}
\Delta v_i = {v_i}^{(1)} - {v_i}^{(0)} &= \Delta v_j + 2\mathrm{Re}(\bar{z}_{ij}\Delta S_{ij}) - |z_{ij}|^2\Delta i_{ij} \\
&\ge 0.
\end{aligned} \tag{23}$$

Therefore, the voltage is increasing, which supports the first inequality in (21). The first inequality in (20) is due to the property of $\hat{S}_{ij} = \hat{P}_{ij} + j\hat{Q}_{ij}$. The second inequality in (20) is due to (17).

It is not difficult to verify that for $k \ge 2$, (19)–(23) are valid. Notice that $v^{(k)} \le \hat{v} \le \bar{v}$, the new series will be,

$$\begin{aligned}
&\{S^{(k)}\} : S^{(0)} \le S^{(1)} \le S^{(2)} \le \cdots \le \hat{S}, \\
&\{i^{(k)}\} : i^{(0)} \ge i^{(1)} \ge i^{(2)} \ge \cdots \ge 0, \\
&\{{s_0}^{(k)}\} : {s_0}^{(0)} \ge {s_0}^{(1)} \ge {s_0}^{(2)} \ge \cdots \ge \hat{s}_0, \\
&\{v^{(k)}\} : v^{(0)} \le v^{(1)} \le v^{(2)} \le \cdots \le \hat{v}.
\end{aligned}$$

Therefore, the above series have limits and the limits satisfy the constraints of the OPF. Moreover, the SOCP is exact. This ends the proof of Proposition 3.

C. Discussion on Sufficient Condition A1, B1 and C1

The sufficient condition proposed in [13], named as B1, is rewritten in this paper.

B1: The positive linear approximation of the reverse power based on the upper limit of the sub-inject $\bar{s}$ fulfils (24), and the linear approximation of the voltage based on the sub-injection s fulfils (18)

$$A_{i_1}A_{i_2}A_{i_3}\ldots A_{i_{n-1}}u_{i_n} > 0 \quad \forall i_1 \sim i_n, i_1 > 0, \tag{24}$$

where i_x is the parent node of i_{x+1},

$$A_i = I - \frac{2}{v_i}\begin{pmatrix} r_i \\ x_i \end{pmatrix}\left((\hat{P}_i(\bar{p}))^+ (\hat{\mathrm{Q}}_i(\bar{q}))^+\right),$$

$u_i = \binom{r_i}{x_i}$, i represents $i_1 \sim i_n$, symbol a^+ means$\max(a, 0)$.

It can be seen that A1 is a special case of B1 given that $r, x > 0$. According to A1, $\bar{s} \le 0$. There are $(\hat{P}_i(\bar{p}))^+ = 0$ and $(\hat{\mathrm{Q}}_i(\bar{q}))^+ = 0$. Therefore, $A_i = I$ and the left side of (24) equals

to u_i, which is strictly positive since $r, x > 0$. Equation (18) is also satisfied because $\hat{v} \leq 0 < \bar{v}$.

A1 is also a special case of C1. Since $\bar{s} \leq 0$, there is $s \leq 0$. Therefore, $\hat{S} \leq 0$ and the left side of (17) is always negative. Equation (18) is satisfied because $\hat{v} \leq 0 < \bar{v}$. Comparing to A1, C1 allows active reverse power flow or reactive reverse power flow while A1 does not allow any reverse power flow.

The differences between B1 and C1 are analyzed below. First of all, it should be emphasized that B1 is a sufficient condition for the exactness of the SOCP without line flow constraints while C1 is proposed for the case with line flow constraints.

Secondly, for B1 to be a sufficient condition, the cost function f_0 is required to be strictly increasing, while for the case with C1, it only needs to be non-decreasing.

Thirdly, there is no requirement of the impedance for C1 (and A1 as well), but it is required that $r, x > 0$ for B1. This is because the "greater than" symbol is used in (24).

At last, B1 does not imply C1 and vice versa. According to B1, the reverse power flow has an obvious upper limit, $\hat{P}_i(\bar{p}) < \frac{v_i}{2r_i}$ and $\hat{Q}_i(\bar{q}) < \frac{v_i}{2x_i}$, due to (24) and the definition of. However, according to C1, if the active power flow is very high, the allowed reactive reverse power flow will also be very high, without an explicit upper limit. On the other hand, B1 may allow both active and reactive reverse power flowA_i at the same time. However, C1 does not allow both active and reactive reverse power flow at the same time.

IV. AC OPF for Multi-Period EV Energy Planning

In this section, the AC OPF with EV charging planning over multi-period is described considering the line flow and voltage limits

$$\mathbf{OPF-EV}: \min_{e,s,S,v,i,s_0} g = \sum_{t\in\mathcal{T}} (c_t \sum_{k\in\mathbb{V}} e_k) \tag{25}$$

s.t.

$$S_{ijt} = s_{it} + \sum_{h:h\to i} (S_{hit} - z_{hi} i_{hit}), \quad \forall (i,j) \in \mathcal{E}, t \in \mathcal{T} \tag{26}$$

$$0 = s_{0t} + \sum_{h:h\to 0} (S_{h0t} - z_{h0} i_{h0t}), \quad \forall t \in \mathcal{T} \tag{27}$$

$$v_{it} - v_{jt} = 2\mathrm{Re}(\bar{z}_{ij} S_{ijt}) - |z_{ij}|^2 i_{ijt}, \quad \forall (i,j) \in \mathcal{E}, t \in \mathcal{T} \tag{28}$$

$$i_{ijt} = \frac{|S_{ijt}|^2}{v_{it}}, \quad \forall (i,j) \in \mathcal{E}, t \in \mathcal{T} \tag{29}$$

$$i_{ijt} \leq \bar{i}_{ij}, \quad \forall (i,j) \in \mathcal{E}, t \in \mathcal{T} \tag{30}$$

$$|S_{ijt}| \leq \bar{S}_{ij}, \quad \forall (i,j) \in \mathcal{E}, t \in \mathcal{T} \tag{31}$$

$$\underline{v}_i \leq v_{it} \leq \bar{v}_i, \quad \forall i \in \mathcal{N}^+, t \in \mathcal{T} \tag{32}$$

$$\mathrm{Re}(s_{it}) = -\sum_{k\in\mathbb{V}_i} e_{kt} - \mathrm{Re}(b_{it}), \quad \forall i \in \mathcal{N}^+, t \in \mathcal{T} \tag{33}$$

$$\mathrm{Im}(s_{it}) = -\mathrm{Im}(b_{it}), \quad \forall i \in \mathcal{N}^+, t \in \mathcal{T} \tag{34}$$

$$\sum_{t\in\mathcal{T}_i} e_{kt} = d_k, \quad \forall\, k \in \mathbb{V} \tag{35}$$

$$0 \leq e_{kt} \leq \bar{e}_k a_{kt}, \quad \forall k \in \mathbb{V}, t \in \mathcal{T}. \tag{36}$$

The objective function is to minimize the total charging cost for the EVs. The EV charging related constraints (33)–(36) are all linear. Only (35) is coupling the multiple periods, which is to satisfy the total charged energy required by each EV. Constraint (36) is to limit the charging power, which will lead to the limit of s_{it} through (33). Because of (29), the OPF-EV problem is nonconvex, which is very hard to solve. Similar to the method employed in the single period OPF, (29) can be relaxed. The corresponding SOCP is written below.

SOCP-EV: (25) s.t. (26)–(28), (30)–(36), and

$$i_{ijt} \geq \frac{|S_{ijt}|^2}{v_{it}}, \quad \forall (i,j) \in \mathcal{E}, t \in \mathcal{T}. \tag{37}$$

Proposition 4: The SOCP-EV is exact if C1 holds.

Proof: Let (e^*, s^*) be an optimal solution of the SOCP-EV, and g^* is the optimal value. For any given period t, the corresponding sub-injection s_t^* can be used to construct a feasible power flow solution, denoted as $(S_t^*, v_t^*, i_t^*, s_{0t}^*)$, to the OPF-EV that satisfies the constraints (26)–(32). Therefore, the solution $(e^*, s^*, S^*, v^*, i^*, s_0^*)$ is feasible to the OPF-EV. It is obvious that the objective value for the OPF-EV based on this feasible solution is also equal to g^*. Hence, g^* is the optimal value of the OPF-EV because g^* is a lower bound of the optimal value due to the relaxation. This ends the proof of Proposition 4. Notice that, B1 cannot be used to determine whether the SOCP-EV is exact, not only because there are line flow constraints (30) and (31), but also there is no f_0.

In some application cases with different market and business assumptions, the line losses are considered in the cost function. Then the objective function (25) can be replaced with the following function.

$$g = \sum_{t\in\mathcal{T}} c_t \mathrm{Re}(s_{0t}). \tag{38}$$

For these applications, a conclusion similar to Proposition 4 can be drawn. The proof is not difficult and is neglected for brevity.

V. Case Studies

Case studies were conducted using the Danish driving pattern and the Bus 4 distribution system of the Roy Billinton Test System (RBTS) [23] and the IEEE 123 node feeder [24]. The details of the case studies are presented in this section.

A. Grid Data

The single line diagram of the Bus 4 distribution network is shown in Fig. 3. Line segments and nodes of the feeder one are labeled in Fig. 3, among which L2-1, L4-3, L6-5, L8-7, L9-7, L11-10, and L12-10 refer to the transformers connecting the corresponding load points. Notice that the labelling follows the rules mentioned in Section II-B. The study is focused on this feeder because it has the most diversity among all the feeders: 5 residential load points with different peak conventional demands and two commercial load points. The detailed data of these load

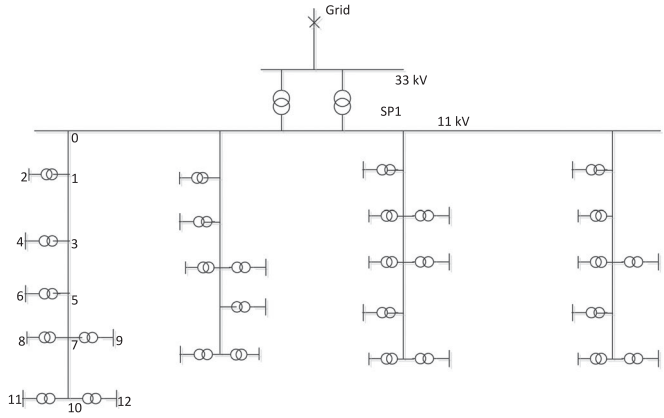

Fig. 3. Single line diagram of the distribution network.

TABLE I
LOAD POINT DATA

Load points	Customer type	Peak conv. load/point (kW)	peak conv. load/point (kVar)	Number oft customers per point
Node 2, 4, 6, 8	Residential	886.9	88.69	200
Node 9	Residential	813.7	81.37	200
Node 11, 12	Commercial	671.4	67.14	10

TABLE II
LINE PARAMETERS

From	To	r (ohm)	x (ohm)	x/r ratio	Capacity limit (kVA)
1	0	0.176	0.52	2.954	8000
2	1	0.4	2.4	6	1000
3	1	0.22	0.66	3	6100
4	3	0.4	2.4	6	2000
5	3	0.264	0.64	2.424	6000
6	5	0.4	2.4	6	2000
7	5	0.176	0.56	3.181	6000
8	7	0.4	2.6	6.5	2000
9	7	0.48	2.8	5.833	2000
10	7	0.22	0.6	2.727	6000
11	10	0.4	2.44	6.1	2000
12	10	0.44	2.8	6.363	2000

points are listed in Table I. The reactive power consumption is assumed to be 10% of the active power consumption for each load point. The peak conventional demands of residential customers occur at 18:00 when people come home and start cooking (shown in Fig. 6).

Voltage limits are set to be $\pm\%$ p.u., then the limits of the square voltage will be $\underline{v} = 0.95^2$ and $\bar{v} = 1.05^2$. Assume that $v_0 = 1$. The line parameters including resistance, reactance and line capacity limits can be seen in Table II. The prices for the EV charging are the predicted day-ahead market system price, as shown in Fig. 4.

B. EV Data

Assume there are 1000 EVs in the network, i.e., one EV per residential customer. The key parameters of the EVs are listed in Table III. The EV availability (available for charge per hour) shown in Fig. 5 is from the driving pattern study in [25].

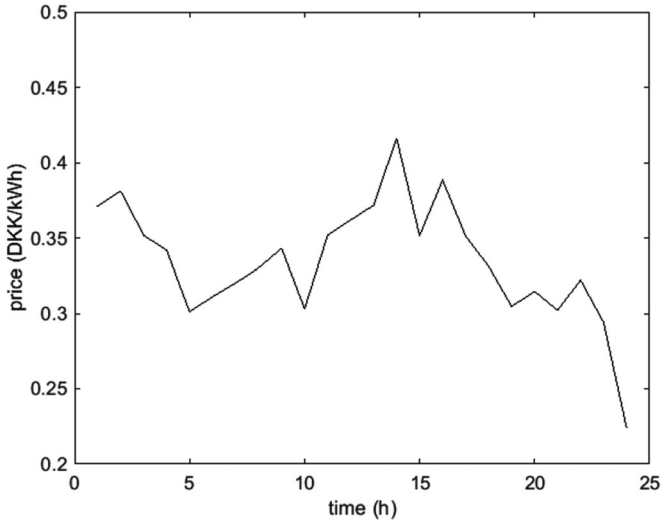

Fig. 4. System prices and DLMPs at LP1.

TABLE III
KEY PARAMETERS OF EVS ([25])

Parameter	Value
EV battery size	25 kW·h
Peak charging power	11 kW (3 phase)
Energy consumption per km	150 W·h/km
Minimum SOC	20%
Maximum SOC	85%
Average driving distance	40 km

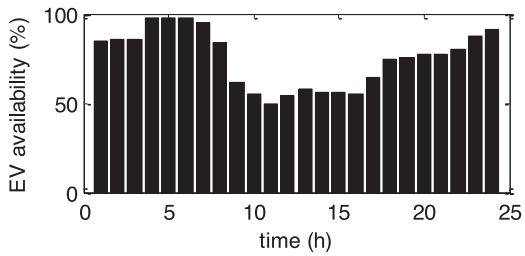

Fig. 5. EV availability.

C. Case Study Results

The simulation is carried out using CVX, a package for specifying and solving convex programs [26], [27]. CVX is a toolbox in MATLAB and it supports several SOCP solvers, such as SeDuMi, SDPT3, Gurobi and MOSEK. In this paper, CVX/MOSEK is chosen, and the platform is a personal computer (a laptop) with Intel Core i5-4310U, 2 GHz, 8GB RAM, windows 64-bit Operation System.

CVX can transform constraints (31) and (37) in SOCP-EV to conic ones, and thereby solved by the SOCP solvers. The optimal solution of the OPF-EV can be recovered using the

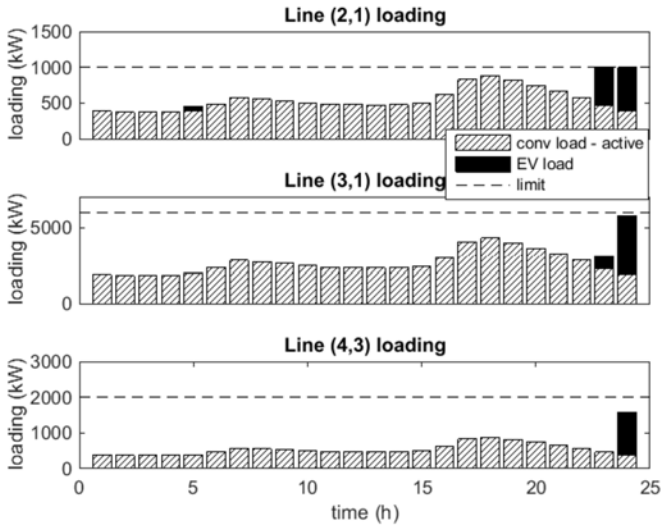

Fig. 6. Active power sharing of EV and conventional loads (active power losses are very small).

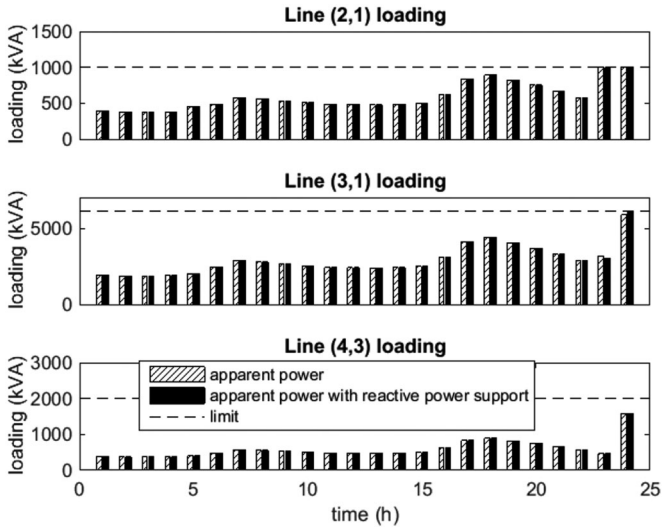

Fig. 7. Apparent power of three line segments.

Forward-Backward sweep method and used to describe the operation status of the network, as shown in Figs. 6–8.

It can be seen from Fig. 6 that most of the EV charging loads are allocated at the hour with the lowest price, i.e., hour 24. However, due to the availability and the line capacity limit, part of the loads is allocated to the hours with the second and third lowest prices. Due to small resistances, the line losses are very small, which is about 1%. Hence, it is not shown in the figure. The sharing of EV loads and conventional loads are calculated using the linear model, i.e. (15), and the losses are the gaps between the linear model and the full model.

The apparent power (magnitude) profile of three line segments is shown in Fig. 7. It can be seen that the apparent power is below or equal to the line capacity limit. Due to the heavy EV charging loads, the capacity limit of L2-1 is reached at hour 23 and hour 24. The apparent power of L3-1 is below the capacity

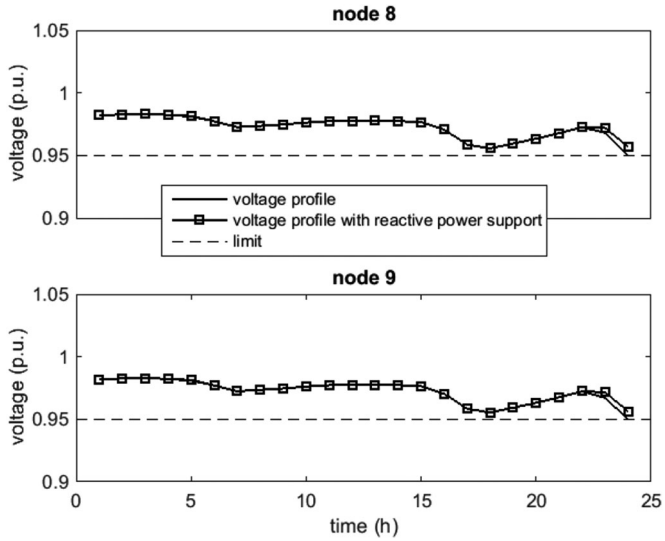

Fig. 8. Voltage profiles of node 8 and 9, which are critical node in the feeder.

TABLE IV
SOCP-EV MODEL EFFICIENCY TEST

Simulation	1	2	3
Number of nodes (exclude root)	12	50	123
Number of EVs	1000	4000	20 000
Constraints	3280	13 576	43 592
Cones	576	2400	5904
Scalar variables	28 217	113 249	532 521
Time (s)	0.39	1.56	12.09

limit at hour 24 because the voltage limit is hit first as shown in Fig. 8.

A second case study was carried out, where the EVs were allowed to produce reactive power up to 10% of its active power, to test the reactive power support function of the EVs and the validity of C1. With the feed-in of reactive power, the voltage profile is improved (see Fig. 8), and the total cost is reduced a bit because the EVs are able to consume more energy at the lowest price up to the limit of the line capacity as shown in Fig. 7.

At last, the efficiency of the SOCP-EV model was tested on distribution networks of different complexity scales. The results were tabularized in Table IV. The first simulation is the case described above. The simulation focuses on the first feeder of the network shown in Fig. 3. The 11 kV bus was deemed as the root node. Because it is a multi-period optimal planning problem, the number of scalar variables depends on the number of EVs and the number of planning periods (24 here). The optimizer only took 0.39 seconds to finish the optimization. The second simulation was done on the whole distribution network. The 33 kV bus was deemed as the root node. The optimizer took 1.56 seconds to finish the optimization. The third simulation was done with the IEEE 123 node test feeder [24]. The number of EVs was increased to 20000 and the total optimization time is 12.09 seconds for such a complicated feeder with high penetration of EVs.

VI. Conclusion

This paper has proven that if A1 holds, i.e., there is no net injection power, the sub-injection region will be convex. Moreover, if the cost function is non-decreasing, the convex relaxation of the AC OPF of distribution networks with line constraints will be exact under A1. When this condition holds, the NP-hard AC OPF of distribution networks can be solved through an SOCP. In order to expand the applicability of the convex relaxed AC OPF in distribution networks with line constraints as an SOCP, a weaker condition C1 is proposed and proved, which allows that the reverse power flow is only active or reactive, or none. The case study demonstrates the exactness of the convex relaxed AC OPF and the efficacy of using the convex relaxed AC OPF for solving a multi-period EV planning problem with line constraints. In the future work, the sufficient condition for the applications with both active and reactive power injections will be studied, which will allow the convex relaxation to solve the AC OPF in much wider applications.

References

[1] H. Dommel and W. Tinney, "Optimal power flow solutions," *IEEE Trans. Power App. Syst.*, vol. PAS-87, no. 10, pp. 1866–1876, Oct. 1968.

[2] B. Stott, J. Jardim, and O. Alsac, "DC power flow revisited," *IEEE Trans. Power Syst.*, vol. 24, no. 3, pp. 1290–1300, Aug. 2009.

[3] R. E. Rosenthal. (Aug. 2014), GAMS—A user's guide. GAMS Development Corporation, Washington, DC, USA. [Online]. Available: http://www.gams.com/dd/docs/bigdocs/GAMSUsersGuide.pdf

[4] W. Min and L. Shengsong, "A trust region interior point algorithm for optimal power flow problems," *Int. J. Electr. Power Energy Syst.*, vol. 27, no. 4, pp. 293–300, May 2005.

[5] A. A. Sousa, G. L. Torres, and C. A. Canizares, "Robust optimal power flow solution using trust region and interior-point methods," *IEEE Trans. Power Syst.*, vol. 26, no. 2, pp. 487–499, May 2011.

[6] E. Baptista, E. Belati, and G. Dacosta, "Logarithmic barrier-augmented Lagrangian function to the optimal power flow problem," *Int. J. Electr. Power Energy Syst.*, vol. 27, no. 7, pp. 528–532, Sep. 2005.

[7] R. A. Jabr, "A primal-dual interior-point method to solve the optimal power flow dispatching problem," *Optim. Eng.*, vol. 4, no. 4, pp. 309–336, Dec. 2003.

[8] R. A. Jabr, "Radial distribution load flow using conic programming," *IEEE Trans. Power Syst.*, vol. 21, no. 3, pp. 1458–1459, Aug. 2006.

[9] X. Bai, H. Wei, K. Fujisawa, and Y. Wang, "Semidefinite programming for optimal power flow problems," *Int. J. Electr. Power Energy Syst.*, vol. 30, no. 6/7, pp. 383–392, Jul. 2008.

[10] J. Lavaei and S. H. Low, "Zero duality gap in optimal power flow problem," *IEEE Trans. Power Syst.*, vol. 27, no. 1, pp. 92–107, Feb. 2012.

[11] B. Zhang and D. Tse, "Geometry of feasible injection region of power networks," in *Proc. 49th Annu. Allerton Conf. Commun., Control, Comput.*, 2011, pp. 1508–1515.

[12] B. Zhang and D. Tse, "Geometry of injection regions of power networks," *IEEE Trans. Power Syst.*, vol. 28, no. 2, pp. 788–797, May 2013.

[13] L. Gan, N. Li, U. Topcu, and S. H. Low, "Exact convex relaxation of optimal power flow in radial networks," *IEEE Trans. Autom. Control*, vol. 60, no. 1, pp. 72–87, Jan. 2015.

[14] B. C. Lesieutre, D. K. Molzahn, A. R. Borden, and C. L. DeMarco, "Examining the limits of the application of semidefinite programming to power flow problems," in *Proc. 49th Annu. Allerton Conf. Commun., Control, Comput.*, 2011, pp. 1492–1499.

[15] B. Biegel, P. Andersen, J. Stoustrup, and J. Bendtsen, "Congestion management in a smart grid via shadow prices," in *Proc. 8th IFAC Symp. Power Plant Power Syst. Control*, 2012, pp. 518–523.

[16] S. Huang, Q. Wu, S. S. Oren, R. Li, and Z. Liu, "Distribution locational marginal pricing through quadratic programming for congestion management in distribution networks," *IEEE Trans. Power Syst.*, vol. 30, no. 4, pp. 2170–2178, Jul. 2015.

[17] S. H. Low, "Convex relaxation of optimal power flow—Part I: Formulations and equivalence," *IEEE Trans. Control Netw. Syst.*, vol. 1, no. 1, pp. 15–27, Mar. 2014.

[18] S. H. Low, "Convex relaxation of optimal power flow—Part II: Exactness," *IEEE Trans. Control Netw. Syst.*, vol. 1, no. 2, pp. 177–189, Jun. 2014.

[19] M. Farivar and S. H. Low, "Branch flow model: Relaxations and convexification—Part I," *IEEE Trans. Power Syst.*, vol. 28, no. 3, pp. 2554–2564, Aug. 2013.

[20] O. Sundstrom and C. Binding, "Planning electric-drive vehicle charging under constrained grid conditions," in *Proc. Int. Conf. Power Syst. Technol.*, 2010, pp. 1–6.

[21] O. Sundstrom and C. Binding, "Flexible charging optimization for electric vehicles considering distribution grid constraints," *IEEE Trans. Smart Grid*, vol. 3, no. 1, pp. 26–37, Mar. 2012.

[22] M. E. Baran and F. F. Wu, "Optimal capacitor placement on radial distribution systems," *IEEE Trans. Power Del.*, vol. 4, no. 1, pp. 725–734, Jan. 1989.

[23] R. N. Allan, R. Billinton, I. Sjarief, L. Goel, and K. S. So, "A reliability test system for educational purposes-basic distribution system data and results," *IEEE Trans. Power Syst.*, vol. 6, no. 2, pp. 813–820, May 1991.

[24] IEEE PES, Distribution test feeders. [Online]. Available: http://ewh.ieee.org/soc/pes/dsacom/testfeeders/index.html, accessed in 2016.

[25] Q. Wu, A. H. Nielsen, J. Østergaard, F. Marra, and C. Træholt, "Driving pattern analysis for electric vehicle (EV) grid integration study," in *Proc. IEEE PES Innovative Smart Grid Technol. Conf. Eur.*, 2010, pp. 1–6.

[26] CVX Research Inc., (Aug. 2012). CVX: MATLAB software for disciplined convex programming, version 2.0. [Online]. Available: http://cvxr.com/cvx/

[27] M. Grant and S. Boyd, "Graph implementations for nonsmooth convex programs," *Recent Advances in Learning and Control*. Berlin, Germany: Springer-Verlag, pp. 95–110, 2008.

Shaojun Huang (S'13) received the B.Eng. degree from the Department of Electrical Engineering, Tsinghua University, Beijing, China, in 2001. He received the M.Sc. degree from the Department of Energy Technology, AAlborg University, Denmark, in 2013.

He is currently working toward the Ph.D. degree at the Centre for Electric Power and Energy, Department of Electrical Engineering, Technical University of Denmark.

His research interests include congestion management for distribution networks with high penetration of distributed energy resources.

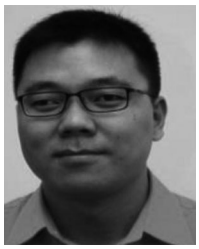

Qiuwei Wu (M'08–SM'15) received the B.Eng. and M.Eng. degrees in power system and automation from the Nanjing University of Science and Technology, Nanjing, China, in 2000 and 2003, respectively. He received the Ph.D. degree in power system engineering from the Nanyang Technological University, Singapore, in 2009.

From March 2008 to October 2009, he worked as a Senior R&D Engineer with the VESTAS Technology R&D Singapore Pte Ltd. Since November 2009, he has been working at the Department of Electrical Engineering, Technical University of Denmark (PostDoc November 2009–October 2010, Assistant Professor November 2010–August 2013, Associate Professor since September 2013). From February 2012 to May 2012, he was a Visiting Scholar at the Department of Industrial Engineering & Operations Research, University of California, Berkeley, funded by the Ministry of Science, Technology and Innovation, Denmark. He is also a Visiting Professor named by Y. Xue, an Academician of the Chinese Academy of Engineering, Shandong University, China. His research interests include integration of wind power and electric vehicle into power systems, active distribution networks, and real time power system simulation and analysis.

Dr. Wu is an Editor of IEEE Transactions on Smart Grid and IEEE Power Engineering Letters.

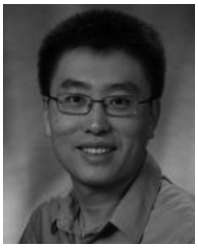

Jianhui Wang (M'07–SM'12) received the Ph.D. degree in electrical engineering from the Illinois Institute of Technology, Chicago, IL, USA, in 2007.

He is currently the Section Lead for Advanced Power Grid Modeling at the Energy Systems Division, Argonne National Laboratory, Argonne, IL, USA. He is also an Affiliate Professor at Auburn University and an Adjunct Professor at the University of Notre Dame.

Dr. Wang is the Secretary of the IEEE Power & Energy Society (PES) Power System Operations Committee. Before being promoted and elected to this position, he was the Chair of the IEEE PES Power System Operation Methods Subcommittee for six years. He is the Editor-in-Chief of IEEE TRANSACTIONS ON SMART GRID, an editor of the IEEE TRANSACTIONS ON POWER SYSTEMS, an Associate Editor of the *Journal of Energy Engineering*, an editor of the IEEE PES Letters, and an Associate Editor of *Applied Energy*. He is an IEEE PES Distinguished Lecturer.

Haoran Zhao (S'12–M'15) received the B.E. degree in electrical engineering and automation from the Shandong University, Jinan, China, in 2005, the M.E. degree in electrical engineering and automation from the Technical University of Berlin, Berlin, Germany, in 2009, and the Ph.D. degree in electrical engineering from the Technical University of Denmark, Kgs. Lyngby, Denmark, in 2015.

He is a Postdoctoral Researcher at the Center for Electric Technology, Technical University of Denmark. He worked as an Electrical Engineer with the State Grid Corporation of China, Beijing, China, in 2005. From August 2010 to September 2011, he worked as an Application Developer with DIgSILENT GmbH, Gomaringen, Germany. His research interests include modeling and integration study of wind power, control of energy storage system, and voltage stability analysis.